

Cite this: *RSC Adv.*, 2015, 5, 97036

Surface characterisation of phosphine and phosphite stabilised Rh nanoparticles: a model study†

Jessica Llop Castelbou,^a Pascal Blondeau,^b Carmen Claver^{*a} and Cyril Godard^{*a}

Small and well defined Rh nanoparticles (<2 nm) stabilised by the model ligands triphenylphosphine **1** and triphenylphosphite **2** were synthesised using various P/Rh ratios. In all cases, the crystalline NPs exhibited a spherical shape and a fcc structure. During the synthesis of these materials, hydrogenation and oxidation of the stabilisers take place and the degree of hydrogenation of the stabilising ligand increased when low ligand to Rh ratio is used during their synthesis. The **Rh1** systems mainly contain adsorbed phosphine oxide species at their surface whereas the **Rh2** systems include both phosphite and phosphite oxide species. Analysis of the surface of these nanoparticles by infrared spectroscopy revealed the presence of Rh-H at the surface of the NPs and hydride titration experiments revealed a higher hydride coverage for the phosphine stabilized systems. By CO adsorption/infrared experiments, bridging, terminal and geminal Rh(CO)₂ sites were detected. All these systems were active catalysts in the hydrogenation of styrene and the observation of Rh(CO)₂ sites could be correlated with the activity of these species for the hydrogenation of the aromatic ring.

Received 19th October 2015
Accepted 4th November 2015

DOI: 10.1039/c5ra21835g

www.rsc.org/advances

Introduction

Phosphorus based ligands such as phosphines and phosphites have been extensively and successfully used in homogeneous catalysis due to their rich coordination chemistry and their influence on the stability and selectivity of transition metal catalysts.¹ The ability to finely tune the properties of the catalyst by selecting the adequate steric and electronic features of the ligands is a key tool in homogeneous catalysis for the rational design of new catalysts.²

In recent years, phosphorus based ligands also revealed to efficiently stabilise transition metal nanoparticles (NPs) that are active catalysts in several processes such as arene hydrogenation and CC bond formation.^{3–8} In heterogeneous catalysis, however, the tuning of the catalyst is usually attempted through the use of additives such as thiols⁹ but remains mainly dependant on the size of the particles.¹⁰ Furthermore, in contrast with homogeneous systems where spectroscopic methods can provide information on where and how the ligands are coordinated to the metal centre, the characterisation of these nanocatalysts at the atomic level is much more challenging.¹¹ In view

of the potential of metal nanoparticles in catalysis, there is a need for a better understanding how the ligands stabilise the NPs and affect their surface properties. Recently, the group of Chaudret and co-workers demonstrated that combined IR and NMR spectroscopic studies can allow the very precise location of carbene ligands at the surface of Ru-NPs.¹² They also looked at the dynamics of adsorbed CO molecules by FTIR spectroscopy and observed that the presence of the bulky diphosphine as stabilisers reduces the mobility of these ligands.¹³ These results indicated that the use of the appropriate ligands as stabilisers could lead to the modulation of the surface properties of M-NPs, and thus open the way to the rational design of selective nanocatalysts. Moreover, Dyson and co-workers showed that the addition of phosphines to Rh-PVP NPs of *ca.* 3 nm of diameter improves the selectivity of these nanocatalysts in hydrogenation reactions.¹⁴ They postulated that the selective coordination of these ligands could modify the steric hindrance at specific sites of the NPs and hence generate selectivity.

In recent years, our research group has reported the application of transition metal nanoparticles in selective catalytic processes using chiral diphosphites as stabilisers.¹⁵ In most cases, the catalytic performances of the resulting catalysts were clearly influenced by the ligands, although no clear structure–reactivity relationship could be achieved. The hydrogenation of substituted arenes was also investigated using soluble Rh-NPs as catalysts, and results showed relevant differences in activity and selectivity depending on the properties of the P-ligand used for the stabilisation of the NPs.⁴ More recently, a study on the behaviour of Ru- and Rh-nanoparticles stabilised by mono- and

^aDepartament de Química Física i Inorgànica, Universitat Rovira i Virgili, C/ Marcel·lí Domingo s/n, Campus Sescelades, 43007, Tarragona, Spain. E-mail: cyril.godard@urv.cat; Fax: +34 977 559563

^bDepartament de Química Analítica i Orgànica, Universitat Rovira i Virgili, C/ Marcel·lí Domingo s/n, Campus Sescelades, 43007, Tarragona, Spain

† Electronic supplementary information (ESI) available. See DOI: 10.1039/c5ra21835g

bidentate phosphines showed clear differences in the selective hydrogenation of aromatic ketones.¹⁶

Herein, we describe the synthesis and characterisation of a series of Rh-NPs stabilised by model monodentate phosphorus donor ligands that are active catalysts in hydrogenation reactions.⁸ Variation of the amount of ligand during the synthesis was performed and CO adsorption-FTIR spectroscopy were used to monitor the effects of the nature of the ligands, their steric bulk and their loading at the surface of the NPs. These features were correlated with the results obtained in the hydrogenation of styrene.

Experimental part

Reagents and general procedures

All syntheses were performed using standard Schlenk techniques under N₂ or Ar atmosphere. Chemicals were purchased from Aldrich Chemical Co, Fluka and Strem. All solvents were distilled over drying reagents and were deoxygenated before use. The precursor [Rh(η^3 -(C₃H₅)₃)]₃, was prepared following previously described methods.²⁷ The synthesis of the nanoparticles were performed using 1L Fisher Porter and pressurized on a high pressure line.

Characterization techniques

TEM experiments were performed at the “Unitat de Microscopia dels Serveis Científicotècnics de la Universitat Rovira I Virgili” (TEM-SCAN) in Tarragona with a Zeiss 10 CA electron microscope operating at 100 kV with resolution of 3 Å. The particles size distributions were determined by a manual analysis of enlarged images. At least 300 particles on a given grid were measured in order to obtain a statistical size distribution and a mean diameter.

XRD measurements were made using a Siemens D5000 diffractometer (Bragg–Brentano parafofocusing geometry and vertical θ – θ goniometer) fitted with a curved graphite diffracted-beam monochromator, incident and diffracted-beam Soller slits, a 0.06° receiving slit and scintillation counter as a detector. The angular 2θ diffraction range was between 26 and 95°. The data were collected with an angular step of 0.05° at 16 s per step and sample rotation. A low background Si(510) wafer was used as sample holder. CuK α radiation was obtained from a copper X-ray tube operated at 40 kV and 30 mA.

XPS experiments were performed in a PHI 5500 Multitechnique System (from Physical Electronics) with a monochromatic X-ray source (Aluminium Kalfa line of 1486.6 eV energy and 350 W), placed perpendicular to the analyser axis and calibrated using the 3d5/2 line of Ag with a full width at half maximum (FWHM) of 0.8 eV. The analysed area was a circle of 0.8 mm diameter, and the selected resolution for the spectra was 187.5 eV of pass energy and 0.8 eV per step for the general spectra and 23.5 eV of pass energy and 0.1 eV per step for the spectra of the different elements in the depth profile spectra. A low energy electron gun (<10 eV) was used in order to discharge the surface when necessary. All measurements were performed in an ultra high vacuum (UHV) chamber pressure between 5×10^{-9} and 2×10^{-8} torr.

TGA experiments were carried out in the furnace of a Mettler Toledo TGA/SDTA851 instrument.

GS-MS spectroscopy was carried out on a HP 6890A spectrometer, with an achiral HP-5 column (0.25 mm \times 30 m \times 0.25 μ m).

General procedure for the synthesis of the Rh-NPs

In a typical procedure, the [Rh(η^3 -C₃H₅)₃] (64 mg, 0.28 mmol) was placed into a Fischer–Porter reactor at –110 °C (acetone/N₂ bath) in 64 ml of dry and deoxygenated THF by freeze–pump–thaw cycles in the presence of the appropriate ligand. The Fischer–Porter reactor was then pressurised under 6 bar of H₂ and stirred for 30 minutes at room temperature. The solution was then heated to 40 °C and stirred at this temperature during 24 h. The initial colourless solution became black after 1 h. A small amount (5 drops approx.) of the solution was deposited under an argon atmosphere on a carbon-covered copper grid for transmission electron microscopy analysis (TEM). The rest of the solution was concentrated under reduced pressure. Precipitation and washing with pentane (3 \times 15 ml) was then carried out, obtaining a black precipitate.

General procedure for the hydrogenation reactions

Autoclave Par 477 equipped with PID control temperature and reservoir for kinetic measurements was used as reactor for the hydrogenation reactions. In a typical experiment, the autoclave was charged in the glove-box with Rh nanoparticles (3.5 mg of Rh-NPs; the catalyst concentration was calculated based on the total number of metallic atoms in the NPs) and the substrate (1.24 mmol, approx. substrate to metal ratio = 55) in 10 ml of heptane. Molecular hydrogen was then introduced until the desired pressure was reached. The reaction was stirred during the corresponding time at 80 °C. The autoclave was then depressurised. The solution was filtered over silica and analysed by gas chromatography. The conversion and the selectivities of the product were determined using a Fisons instrument (GC 9000 series) equipped with a HP-5MS column.

Results and discussion

To evaluate the two model ligands PPh₃ **1** and P(OPh)₃ **2** as stabilisers for Rh-NPs,⁸ the organometallic precursor Rh(η^3 -C₃H₅)₃ was reduced in THF under 6 bar of hydrogen at 40 °C and in the presence of sub-stoichiometric amounts of these ligands (Fig. 1).¹⁷ The amount of P-based stabilisers **1** and **2** was varied from 0.1 to 0.6 equivalent per Rh to study the effect on the formed systems.

Initially, the triphenylphosphine ligand **1** was used to synthesise the series of NPs **Rh1**. The amount of ligand used during the synthesis was varied using 0.1, 0.2, 0.4 and 0.6 equivalent per Rh. However, in the presence of 0.1 equivalent of **1**, no nanoparticles were formed. When the amount of ligand was increased, the NPs **Rh1-0.2**, **Rh1-0.4** and **Rh1-0.6** were formed and isolated.

Interestingly, the TEM micrographs of **Rh1-0.2**–**Rh1-0.6** revealed the formation of very similar nanoparticles with no significant differences in size, shape and distribution since

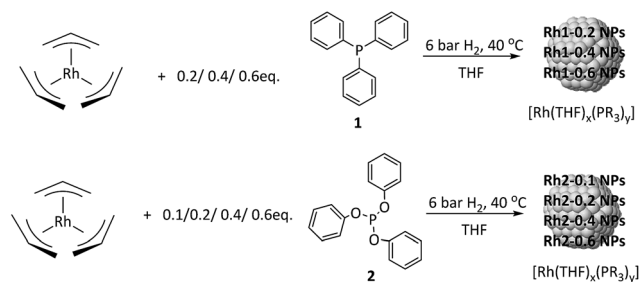


Fig. 1 Synthetic method used for the preparation of the Rh-NPs.

these three systems appeared as spherical NPs with a diameter of $ca. 1.5 \pm 0.2$ nm (Fig. 2). The nanoparticles were characterised by XRD analysis, that revealed crystalline systems with fcc packing. XPS measurements demonstrated that these NPs are mainly constituted by Rh in zero valent state. TGA analysis of these species revealed that **Rh1-0.2** contains 44% in weight of phosphine while for the systems **Rh1-0.4** and **Rh1-0.6**, the values are similar (27% and 30% respectively). In view of these results, no clear correlation could be established between the amount of phosphine **1** used during the synthesis of the nanoparticles and the weight losses observed by TGA.

When the triphenylphosphite ligand **2** was used as stabiliser, the nanoparticles **Rh2-0.1**, **Rh2-0.2**, **Rh2-0.4** and **Rh2-0.6** were obtained using 0.1, 0.2, 0.4 and 0.6 equivalent of ligand **2** per

Rh, respectively (Fig. 1). It is noteworthy that in contrast with the result obtained with **PPh₃** **1**, in the presence of 0.1 eq. of ligand **2** per Rh, the stabilisation of small Rh-NPs was this time efficiently achieved. This result can be explained by the stronger π -acceptor character of the phosphite ligand, which increases its coordinating properties for electron-rich metal centres. The formation of the nanoparticles was confirmed by TEM microscopy and the corresponding micrographs and size distributions are displayed in Fig. 3.

The triphenylphosphite **2** stabilised systems **Rh2-0.1–Rh2-0.6** exhibited similar size and shape with the detection of spherical nanoparticles with diameters of $ca. 1.6 \pm 0.3$ nm. Moreover, no difference in crystallinity nor packing (fcc) was observed by XRD between the systems. Analysis by XPS again showed that these Rh-NPs are mainly constituted by Rh⁰. The systems were also analysed by TGA, revealing that when the

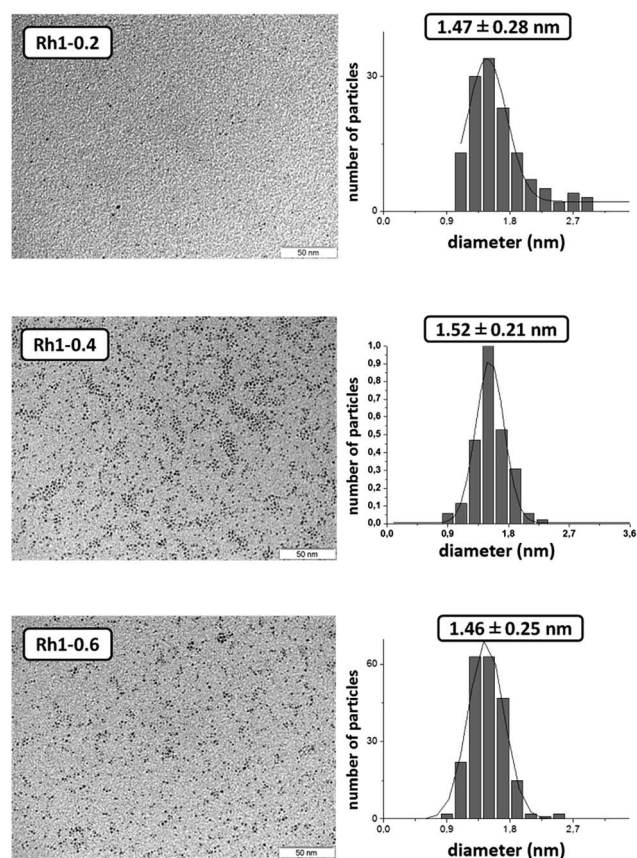


Fig. 2 TEM micrographs and size distributions of the Rh1-0.2, Rh1-0.4 and Rh1-0.6 NPs.

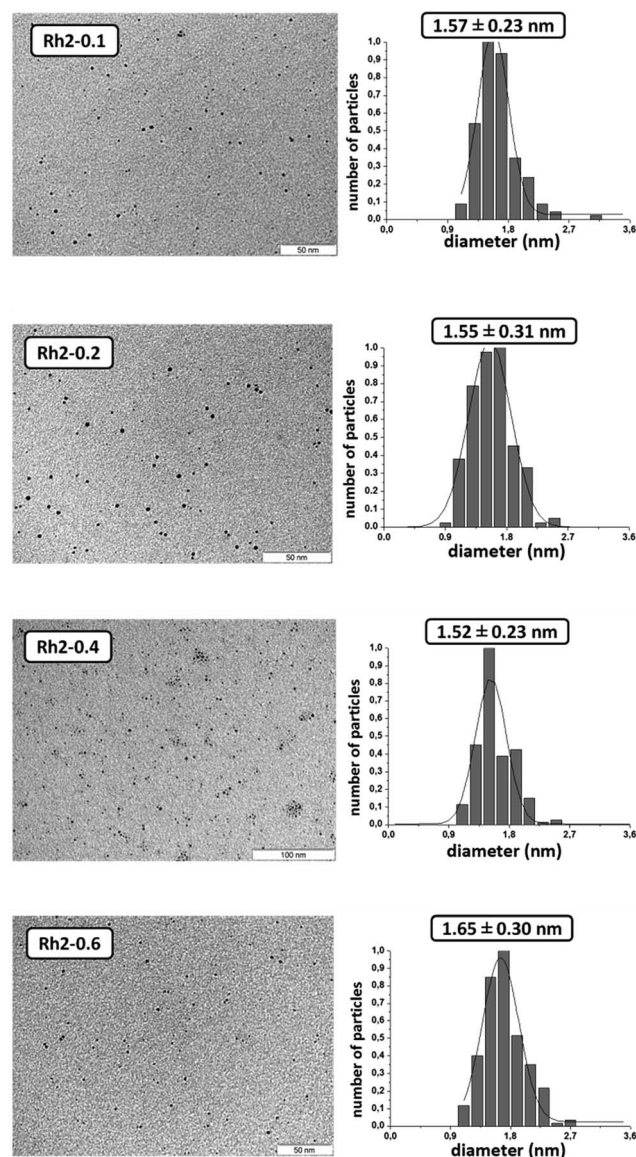


Fig. 3 TEM micrographs and size distributions of the Rh2-0.1, Rh2-0.2, Rh2-0.4 and Rh2-0.6 NPs.

amount of phosphite **2** is increased from 0.1 to 0.6 equivalent during the synthesis of these NPs, an increase in ligand content was observed from 34% for **Rh2-0.1**, 42% for **Rh2-0.2** and **Rh2-0.4**, and 53% for **Rh2-0.6** NPs.

NMR studies

The nanoparticles **Rh1-0.4** and **Rh2-0.4** were analysed by solution NMR spectroscopy in d_8 -THF. For both systems, no signals were detected when the nanoparticles were analysed by ^{31}P NMR at room temperature, as previously described for solution NMR analysis of ligand-stabilised M-NPs and explained by the influence of parameters such as the Knight shift, the fast T2 relaxation resulting from the slow tumbling of the particles in solution and to the surface anisotropy, as described in several reports.^{4,18}

However, when a $^{31}\text{P}\{^1\text{H}\}$ NMR spectrum of the solution containing the system **Rh1-0.4**, was recorded at low temperature (-80°C), a singlet phosphorus signal was detected at 43.3 ppm. This resonance was attributed to diphenylcyclohexylphosphine oxide and confirmed by GC-MS analysis. This observation is in agreement with a recent report that demonstrated the adsorption of phosphine oxide at the surface of Ru-NPs by solid state NMR spectroscopy.¹⁹ This result also indicated that $\text{O}=\text{PCyPh}_2$ is formed from PPh_3 **1** during the NP synthesis *via* hydrogenation of one of the aryl rings and oxidation of the phosphorus centre, or *vice versa*, presumably due to traces of water in the solvent. The non detection of the phosphorus signal at RT also indicated that this phosphine oxide species is involved in a dynamic process between the surface of the NPs and the THF solution. In order to gain information on the species adsorbed at the surface of **Rh1**, the sample was placed in a high pressure sapphire tube and charged with 30 bar of CO pressure at room temperature. In the corresponding $^{31}\text{P}\{^1\text{H}\}$ spectrum, the signal previously detected at low temperature was again observed at 43.3 ppm but with higher intensity and together with three other singlet signals at 37.7, 27.4 and 21.6 ppm. Interestingly, no signal for PPh_3 **1** was detected, which indicated that no untransformed ligand remained after the NP synthesis.

For the system **Rh2-0.4** stabilised by triphenylphosphite **2**, the low temperature (-80°C) spectrum showed a signal at -16 ppm, assigned to triphenylphosphite oxide and indicated that this species was adsorbed at the NP surface and is involved in a dynamic process between the NP surface and the solution. After exposure of the sample to 30 bar of CO pressure, new singlet signals at 1.15 and 7.02 ppm attributed to oxidised derivatives of the stabilising ligand **2** were detected. Moreover, two very broad resonances centred at *ca.* 120 and 135 ppm were also observed. In view of their chemical shifts, these latter signals were attributed to phosphite ligands and the broadness of these signals could indicate a dynamic process involving the P centres of these ligands and the surface of the nanoparticles. These signals were attributed to partially hydrogenated phosphite ligands. It was therefore concluded that when the phosphite **2** is used as stabiliser, the resulting nanoparticles are covered by a mixture of partially hydrogenated phosphite and phosphite oxide ligands.

Therefore, when these NPs are placed under CO pressure, several P-based species adsorbed at their surface are expelled from the NP surface and could be consequently detected by NMR in solution. The system **Rh1-0.4** thus mainly contains diphenylcyclohexylphosphine oxide adsorbed at its surface, together with other phosphine oxides. In the case of **Rh2-0.4**, both phosphite and oxidised phosphite species are adsorbed at their surface.

IR studies

Next, the nanoparticles stabilised with triphenylphosphine **1** were analysed by infrared spectroscopy using a KBr pellet (see spectra in Fig. S22, ESI†). First, the C–H stretching vibrations zone (*ca.* 3000 cm^{-1}) was analysed and compared to that of the ligand **1**. For the nanoparticles **Rh1-0.2** (spectra b) only one set of signals were detected at low frequencies ($2900\text{ cm}^{-1} < \nu < 3000\text{ cm}^{-1}$) attributed to the alkyl $\nu(\text{C-H})$ signals. However, for the system **Rh1-0.4**, a small signal attributed to aromatic $\nu(\text{C-H})$ was observed at higher frequencies ($>3000\text{ cm}^{-1}$). Similar pattern was observed for system **Rh1-0.6** (spectra d), signals of both alkylic and aromatic C–H bonds were observed. It was therefore concluded hydrogenation of the phenyl rings of the ligand had taken place during the synthesis of the NPs, in agreement with the NMR results obtained with the NPs **Rh1-0.4** in solution. Furthermore, the intensity of the aromatic C–H bond stretching signals increased when more ligand is used during synthesis, indicating a higher degree of hydrogenation at lower ligand to Rh ratio. These observations are in agreement with results reported for Ru-NPs stabilized by monodentate ligands.³ At *ca.* 2000 cm^{-1} , a very weak band was observed for system **Rh1-0.2**. This signal was more pronounced in the spectrum of **Rh1-0.4** and **Rh1-0.6**. Such a frequency typically corresponds to carbon monoxide ligands coordinated in terminal mode to a metal centre or a metal surface²⁰ or a metal hydride stretching. For instance, in a study on Rh/ Al_2O_3 catalyst under H_2 , Worley and co-workers attributed a similar band at 2013 cm^{-1} to rhodium hydride species.²¹ To confirm the identity of these species, the authors repeated the reaction under D_2 , observing the disappearance of this band and the detection of a new signal at 1441 cm^{-1} .

Therefore, a fresh sample of **Rh1-0.4** was synthesised under D_2 as instead of H_2 and an IR spectrum of **Rh1-0.4-D₂** was recorded (see Fig. S23, spectrum c *vs.* a, ESI†). In this spectrum, the intense band previously observed at 1973 cm^{-1} was not detected, clearly indicating that this stretching was arising from a Rh-hydride moiety. However, in our case, the displacement of this band to lower frequencies could not be observed due to overlapping with other signals. It was therefore concluded from these observations that the signal observed at 1973 cm^{-1} arises from the presence of Rh-H species at the surface of the NPs.

When the 4 sets of nanoparticles **Rh2** stabilised by the triphenylphosphite **2** were analysed by IR spectroscopy, similar results than with **Rh1** were obtained.

Comparing the spectra of **Rh2-0.1–Rh2-0.6**, no relevant differences were observed, except for the C–H stretching frequencies at *ca.* 3000 cm^{-1} (Fig. 4). Similarly to the results

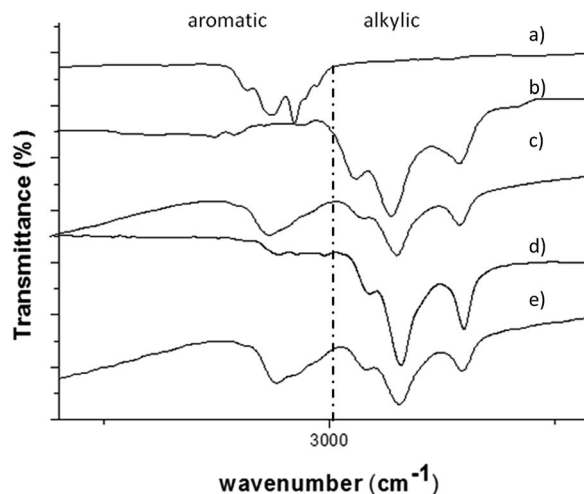


Fig. 4 Selected region of the IR spectra of (a) P(OPh)_3 2, (b) **Rh2-0.1**, (c) **Rh2-0.2**, (d) **Rh2-0.4**, (e) **Rh2-0.6**.

described for PPh_3 1 as stabilizers, complete hydrogenation of the ligand 2 was indicated for **Rh2-0.1** since only aliphatic C–H stretching bands were detected. When higher amount of ligand was used during the synthesis, the detection of both aromatic and aliphatic C–H stretching bands suggested that the reduction of the ligand was only partial.

In agreement with the NMR results, these observations demonstrated that total or partial hydrogenation of the ligand takes place during the synthesis of both sets of nanoparticles **Rh1** and **Rh2**.

Moreover, the spectra of **Rh2** exhibited a small and broad band at 1999 cm^{-1} . When the NPs **Rh2-0.4** were synthesised under D_2 and analysed by IR spectroscopy, the corresponding spectrum did not exhibit such a band (see spectra in Fig. S24, ESI†). This result thus indicated that rhodium hydrides are also present at the surface of the nanoparticles **Rh2**. It is noteworthy that the Rh–H stretching band had a lower intensity in the case of **Rh2-0.4** than for **Rh1-0.4**.

To quantify the amount of Rh hydride present at the surface of **Rh1** and **Rh2**, titration experiments were performed on these nanoparticles following a reported methodology: freshly synthesised samples of **Rh1** and **Rh2** were reacted with norbornene and the quantity of norbornane produced was determined by GC-MS.⁴ The results showed that in the case of the phosphine stabilised systems **Rh1**, *ca.* 0.4, 0.8 and 0.1 mol of hydride per Rh surface atom are present in the systems **Rh1-0.2**, **Rh1-0.4** and **Rh1-0.6** respectively while for the phosphite stabilised nanoparticles **Rh2**, values between 0.15 and 0.3 mol of hydride per Rh surface atom were obtained.

To summarise, the **Rh2-0.4** NPs stabilised by the triphenylphosphite ligand 2 exhibit similar properties than its phosphine counterpart **Rh1-0.4** such as size, shape, and structure packing. Furthermore, NMR and IR studies revealed that hydrogenation and oxidation of the ligands take place during the synthesis of both sets of NPs and that in both cases, Rh–H species are present at the surface of the NPs. The **Rh1-NPs** revealed to contain only oxidised ligands at their surface while

a mixture of both oxidised and unoxidised phosphites are adsorbed at the surface of **Rh2**. Moreover, a higher hydride coverage is present at the surface of the phosphine stabilised **Rh1-NPs** than at that of the phosphite stabilised **Rh2** nanoparticles. It is noteworthy that these values are lower than those reported for related P-ligand stabilised ruthenium nanoparticles of similar size (*ca.* 1.1 mol M–H/Ru surface atom).⁴

To gain further information on the surface of the rhodium nanoparticles, freshly synthesised NPs were reacted in the solid state with 1 atm of CO at room temperature and infrared (IR) spectra of the sample in KBr pellets were recorded.

Initially, a series of samples of **Rh1-0.4** were placed under CO pressure during 2, 4, 6 and 12 h and the resulting samples analysed by IR spectroscopy. The spectra of **Rh1-0.4** exposed to 1 atm of CO after 2, 4 and 6 h were very similar: two large absorptions at 1870 cm^{-1} and 2032 cm^{-1} were observed and attributed to bridging and terminal carbonyl ligands, respectively, in agreement with previously reported measurements (Fig. S25, ESI†).²² As no shift to higher frequency was observed when the time of the CO exposure increased, it was deduced that the total CO coverage had been reached during this time.²³ However, after 12 h of CO exposure, a new band at 2090 cm^{-1} was detected. In previously reported studies on Rh surfaces, such a high frequency band was attributed to one component of the signal for geminal $\text{Rh}(\text{CO})_2$, the other component being detected at *ca.* 2020 cm^{-1} .^{20,21,24} Here, this latter band could not be detected due to the overlapping with the signal centred at 2032 cm^{-1} and corresponding to terminal CO ligands. In order to investigate the effect of CO pressure, the sample **Rh1-0.4** was exposed to 40 bar of CO during 12 h, depressurised and analysed by IR. The high frequency band reported for geminal $\text{Rh}(\text{CO})_2$ was slightly more intense and a shoulder at *ca.* 2000 cm^{-1} was revealed under this conditions, confirming the assignment of these signals (see Fig. S26, ESI†).

These results therefore indicated that CO adsorption on various sites of the NPs **Rh1-0.4** had taken place and evolved with time. During the first 6 h, coordination of CO in bridging (faces) and in terminal mode (apexes and edges) at the surface of the nanoparticles **Rh1-0.4** was observed. At longer reaction times, a geminal $\text{Rh}(\text{CO})_2$ stretching was detected, indicating that adsorption of CO to form these groups is slow compared to initial coordination of CO. It was also shown that the formation of these species is favoured when the sample is exposed to higher CO pressure although the small differences between the spectra after exposure to 1 and 40 bar of CO could indicate that the formation of these species is not very sensitive to CO pressure or that it is a reversible process and that *in situ* experiments are needed to appreciate the corresponding changes.

The detected geminal $\text{Rh}(\text{CO})_2$ can be formed at the apexes and edges of the nanoparticles. It is usually assumed that the stabilising P-based ligands are situated on the apexes of metallic nanoparticles, as demonstrated for the well characterised $\text{Au}_{55}\text{Cl}_6(\text{PPh}_3)_{12}$.²⁵ The Rh atoms in these positions should thus not be able to coordinate to two molecules of CO. However, the displacement of the stabilising agents by CO in the solid state cannot be discarded.

The nanoparticles **Rh1-0.2** and **Rh1-0.6** were placed under CO pressure under the same previously described conditions for **Rh1-0.4** and the results obtained for these systems were compared with those for **Rh1-0.4** NPs (Fig. 5).

In all these spectra, a broad band at *ca.* 1800–1900 cm^{-1} was attributed to bridging carbonyl and a more intense band at 2038 cm^{-1} was related to terminal carbonyls. In the spectrum of **Rh1-0.2**, only these two bands were observed. However, at higher ligand/Rh ratio, the bands corresponding to $\text{Rh}(\text{CO})_2$ were observed to increase in intensity. For **Rh1-0.6**, the bands for these latter sites were clearly detected at 2090 and 2007 cm^{-1} . Furthermore, at higher ligand/Rh ratio, the band for the bridging CO ligands was observed to shift to lower frequency (from 2038 cm^{-1} for **Rh1-0.2** to 2028 cm^{-1} for **Rh1-0.6**) and to decrease in intensity. These observations could indicate that at higher ligand concentration during the NPs synthesis, the stabilising ligands coordinate on the faces of the NPs, resulting in an increase in electron density of the system and a lower CO coverage on these sites, both of which contribute to the lowering of the frequencies for these signals.

Comparing the spectra obtained for the systems **Rh1-0.2**, **Rh1-0.4** and **Rh1-0.6**, a clear trend can be deduced: at higher ligand/Rh ratio, the coordination of the stabiliser on the faces of these NPs and the formation of geminal $\text{Rh}(\text{CO})_2$ sites are favoured. The steric hindrance induced by the presence of the ligands on the faces of the nanoparticles might hamper their coordination on the NP edges and thus enhance the formation of geminal $\text{Rh}(\text{CO})_2$ sites when placed under CO.

Next, the surface analysis of nanoparticles **Rh1-0.4** by CO adsorption-IR spectroscopy as a function of time and with various equivalents of ligand **1** show that both the CO exposure (time and pressure) and the amount of ligand used during synthesis influence the surface environment of these NPs since the formation of $\text{Rh}(\text{CO})_2$ sites was increased at longer exposure, at higher pressure and at higher ligand/Rh ratio.

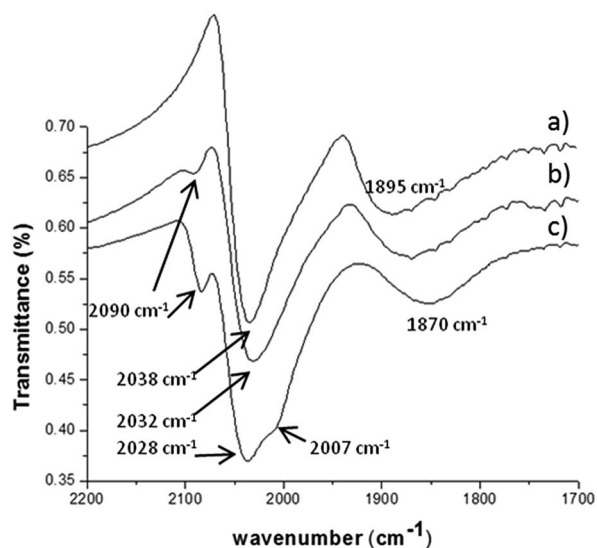


Fig. 5 Carbonyl region of the IR spectra of (a) **Rh1-0.2**, (b) **Rh1-0.4** and (c) **Rh1-0.6** after 12 h under CO atmosphere.

It should be noted that the band previously observed for **Rh1-0.4** at *ca.* 2000 cm^{-1} and attributed to Rh-H at the surface of the NPs could not be detected in these samples. This was attributed to the removal of hydrides under CO exposure, as previously reported.¹³

The same experiments were performed for the systems stabilised with triphenylphosphite **2** ligand. For the **Rh2-0.4** system, the effect of the CO exposure time was monitored at 2, 4, 6 and 12 h (Fig. S27, ESI†). After 2 h of CO exposure, two main signals at 2035 and 2002 cm^{-1} were detected and attributed to terminal carbonyl ligands, together with a very weak band at 1830 cm^{-1} corresponding to bridging COs. Under these conditions, the signals for geminal $\text{Rh}(\text{CO})_2$ were not detected. At longer reaction time, the band for bridging carbonyl was observed to increase in intensity while those for terminal COs remained unchanged. This result indicated that CO could first coordinate to the terminal positions, namely edges and apexes, to later get displaced to bridging positions located at the faces, which is in contrast with previous IR observations on Ru-NPs.²⁶

The IR spectra of **Rh2-0.1–Rh2-0.6** after CO adsorption are displayed in Fig. 6.

Interestingly, the CO bridging bands were found to shift to lower frequency when the ligand coverage increased, as expected for an increase in electronic density of the surface. With this system, a small band at *ca.* 2090 cm^{-1} attributed to a terminal $\text{Rh}-(\text{CO})_2$ stretching was only observed at low P-coverage, indicating that the corresponding position is occupied by the ligand at higher P-content.

This observation contrasts with the results obtained for the system **Rh1** and clearly indicates that the stabilizers **1** and **2** do not coordinate at the NP surface in the same manner.

Catalytic experiments

The nanoparticles previously described were used as catalysts in the hydrogenation of styrene at 80 °C during 16 h. The results are summarised in Table 1.

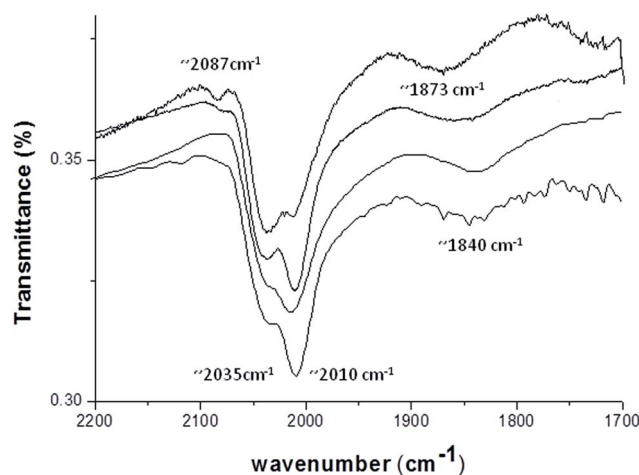
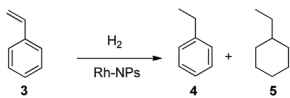


Fig. 6 Carbonyl region of the IR spectra of systems (a) **Rh2-0.1**, (b) **Rh2-0.2**, (c) **Rh2-0.4** and (d) **Rh2-0.6** after CO adsorption.

Table 1 Catalytic hydrogenation of styrene using the Rh-NPs^a


Entry	NPs	% conv. ^b	% 4 ^b	% 5 ^b
1	Rh1-0.2	100	—	100
2	Rh1-0.4	100	—	100
3	Rh1-0.6	100	—	100
4	Rh2-0.1	100	26	73
5	Rh2-0.2	100	87	13
6	Rh2-0.4	100	97	3
7	Rh2-0.6	100	100	0

^a General conditions: 1.24 mmol of substrate, 2 mol% of Rh-NPs, 10 ml of heptane, $T = 80\text{ }^{\circ}\text{C}$, $P = 40\text{ bar H}_2$, $t = 16\text{ h}$. ^b Determined by GC.

In all experiments, full conversion of the substrate was observed. However, the selectivity for ethylbenzene 4 or for the fully hydrogenated product ethylcyclohexane 5 revealed to be strongly affected by the ligand coverage on these catalysts.

When the reaction was carried out using the nanoparticles stabilized with triphenylphosphine 1, only the complete hydrogenation product ethylcyclohexane 5 was observed for all the systems **Rh1-0.2**, **Rh1-0.4** and **Rh1-0.6** (entries 1, 2 and 3).

With the nanoparticles stabilized by triphenylphosphite 2, the selectivity to ethylbenzene 4 was observed to steadily increase when the ligand coverage on the catalyst was increased. When system **Rh2-0.1** was used 73% of product ethylcyclohexane 5 was observed (entry 4), while only 13% and 3% of this product was detected using **Rh2-0.2** and **Rh2-0.4** nanoparticles, respectively (entries 5 and 6). However, 100% selectivity towards the hydrogenation of the vinyl group was reached when **Rh2-0.6** was used, and only ethylbenzene 4 was detected (entry 7). It was therefore concluded that at high ligand coverage, the sites responsible for the hydrogenation of arenes are occupied by the stabilizer and thus, only the vinyl unit of the substrate can be hydrogenated.

CO adsorption-infrared spectroscopy experiments showed that the sites detected as $\text{Rh}(\text{CO})_2$ were occupied by the ligands at high phosphite coverage while these sites were available for CO adsorption at low ligand coverage. A correlation could therefore be deduced between the availability of these sites of the NPs and their ability to hydrogenate the aromatic ring of the substrate.

Conclusions

All the nanoparticles synthesized in this work using triphenylphosphine 1 and triphenylphosphite 2 as stabilisers exhibited a small diameter (<2 nm) with narrow size distributions, a spherical shape and a good dispersion. These crystalline materials exhibit a fcc structure and are mainly constituted by Rh in the zero valent state.

The amount of stabilizer was varied during the synthesis between 0.1 to 0.6 equivalent of ligand per Rh. No variation in size nor shape were observed when this parameter was varied but in both cases, a higher degree of hydrogenation of the stabilising ligand was observed at low ligand to Rh ratio during the synthesis. Furthermore, solution NMR experiments showed that the **Rh1** systems mainly contained adsorbed phosphine oxide species at the surface whereas in the case of the phosphite stabilized NPs **Rh2**, both phosphite and phosphite oxide species could be identified.

Hydride titration experiments were performed on these systems, revealing a higher hydride coverage in the case of the phosphine stabilized systems. Analysis of the surface of these nanoparticles by infrared spectroscopy revealed the presence of a Rh-H stretching band at $1950\text{--}2000\text{ cm}^{-1}$.

CO adsorption/infrared experiments were performed and several conclusions can be drawn:

- Three types of carbonyl signals were observed: bridging ($1800\text{--}1900\text{ cm}^{-1}$), terminal ($1950\text{--}2070\text{ cm}^{-1}$) and geminal $\text{Rh}(\text{CO})_2$ (*ca.* 2100 and 2020 cm^{-1}), associated with the faces, and the apexes and edges of the NPs, respectively.

- For the PPh_3 system **Rh1**, at higher ligand/Rh ratio, the coordination of the stabiliser on the faces is observed and the formation of geminal $\text{Rh}(\text{CO})_2$ sites was favoured. The formation of these $\text{Rh}(\text{CO})_2$ species was also favoured when the sample was exposed to higher CO pressure (40 bar). For the systems stabilised by the triphenylphosphite 2, the opposite trend was observed and increasing the amount of stabilising agent caused the disappearance of the signal for geminal carbonyls $\text{Rh}(\text{CO})_2$. It was concluded that at high ligand/Rh ratio, the corresponding sites are occupied by the ligand.

All these systems were active catalysts in the hydrogenation of styrene. The systems stabilised by triphenylphosphine 1 showed no selectivity as only the complete hydrogenation product ethylcyclohexane 5 was detected using these systems. However, for the triphenylphosphite 2 stabilised systems, the selectivity towards the ethylbenzene 4 product increased at higher ligand/Rh ratio, obtaining 100% selectivity using **Rh2-0.6** nanoparticles. It was therefore concluded that the coordination of the ligand at the site detected as $\text{Rh}(\text{CO})_2$ inhibits the hydrogenation of the aromatic ring.

Acknowledgements

We are grateful to the Spanish Ministerio de Economía y Competitividad for financial support (CTQ2010-14938, CTQ2013-43438-R, CTQ2013-46404-R and 2014 SGR 670, Ramon y Cajal to C. G.)

Notes and references

- 1 J. G. de Vries, *Fine Chemical Synthesis-Homogeneous*, Wiley, 2002.
- 2 P. W. N. M. van Leeuwen, *Homogeneous Catalysis: Understanding the Art*, Kluwer Academic Publishers, Dordrecht, 2004.

- 3 D. Conzález-Gálvez, P. Nolis, K. Philippot, B. Chaudret and P. W. N. M. van Leeuwen, *ACS Catal.*, 2012, **2**, 317–321.
- 4 J. García-Antón, M. R. Axet, S. Jansat, K. Philippot, B. Chaudret, T. Pery, G. Buntkowsky and H.-H. Limbach, *Angew. Chem., Int. Ed.*, 2008, **47**, 2074–2078.
- 5 A. Gual, C. Godard, S. Castillon and C. Claver, *Dalton Trans.*, 2010, **39**, 11499–11512.
- 6 A. Roucoux, J. Schulz and H. Patin, *Chem. Rev.*, 2002, **102**, 3757–3778.
- 7 D. Astruc, F. Lu and J. R. Aranzaes, *Angew. Chem., Int. Ed.*, 2005, **44**, 7852–7872.
- 8 J. Llop Castelbou, A. Gual, E. Mercadé, C. Claver and C. Godard, *Catal. Sci. Technol.*, 2013, **3**, 2828–2833.
- 9 (a) B. J. Hornstein, J. D. Aiken and R. G. Finke, *Inorg. Chem.*, 2002, **41**, 1625–1638; (b) F. Notheisz, A. Zsigmond, M. Bartok, Z. Szegletes and G. V. Smith, *Appl. Catal., A*, 1994, **120**, 105; (c) L. Gonzalez-Tejuca, K. Aika, S. Namba and J. J. Turkevich, *J. Phys. Chem.*, 1977, **81**, 1399.
- 10 (a) G. A. Somorjai, H. Frei and J. Y. Park, *J. Am. Chem. Soc.*, 2009, **131**, 16589–16605; (b) S. M. Humphrey, M. E. Grass, S. E. Habas, K. Niesz, G. A. Somorjai and T. Don Tiley, *Nano Lett.*, 2007, **3**, 785–790.
- 11 (a) D. Astruc, *Nanoparticles and Catalysis*, WILEY-VCH, Weinheim, 2008; (b) For recent papers on atomic level characterization of mono and bimetallic NPs, see for instance: Z. Konuspayeva, P. Afanasiev, T.-S. Nguyen, L. Di Felice, F. Morfin, N.-T. Nguyen, J. Nelayah, C. Ricolleau, Z. Y. Li, J. Yuan, G. Berhault and L. Piccolo, *Phys. Chem. Chem. Phys.*, 2015, **17**, 28112–28120; (c) R. L. Chantry, I. Atanasov, W. Siriwatcharapiboon, B. P. Khanal, E. R. Zubarev, S. L. Horswell, R. L. Johnston and Z. Y. Li, *Nanoscale*, 2013, **5**, 7452–7457.
- 12 (a) P. Lara, O. Rivada-Wheelaghan, S. Conejero, R. Poteau, K. Philippot and B. Chaudret, *Angew. Chem., Int. Ed.*, 2011, **50**, 12080–12084; (b) R. Bronger, T. D. Le, S. Bastin, J. García-Antón, C. Citadelle, B. Chaudret, P. Lecante, A. Igau and K. Philippot, *New J. Chem.*, 2011, **35**, 2653–2660.
- 13 F. Novio, K. Philippot and B. Chaudret, *Catal. Lett.*, 2010, **140**, 1–7.
- 14 D. J. Snelders, N. Yan, G. Laurency and P. J. Dyson, *ACS Catal.*, 2012, **2**, 201–207.
- 15 (a) A. Gual, C. Godard, K. Philippot, B. Chaudret, A. Denicourt-Nowicki, A. Roucoux, S. Castillon and C. Claver, *ChemSusChem*, 2009, **2**, 769–779; (b) A. Gual, R. Axet, K. Philippot, B. Chaudret, A. Denicourt-Nowicki, A. Roucoux, S. Castillon and C. Claver, *Chem. Commun.*, 2008, **24**, 2759–2761.
- 16 J. Llop Castelbou, E. Bresó-Femenia, P. Blondeau, B. Chaudret, S. Castillon, C. Claver and C. Godard, *ChemCatChem*, 2014, **6**, 3160–3168.
- 17 B. Chaudret, *C. R. Phys.*, 2005, **6**, 117–131.
- 18 P. Lara, M.-J. Casanove, P. Lecante, P.-F. Fazzini, K. Philippot and B. Chaudret, *J. Mater. Chem.*, 2012, **22**, 3578–3584.
- 19 T. Gutman, E. Nonefille, H. Breitzke, P.-J. Debouttière, K. Philippot, R. Poteau, G. Buntkowsy and B. Chaudret, *Phys. Chem. Chem. Phys.*, 2013, **15**, 17383–17394.
- 20 A. C. Yang and C. W. Garland, *J. Am. Chem. Soc.*, 1957, **61**, 1504.
- 21 J. P. Wey, W. C. Neely and S. D. Worley, *J. Phys. Chem.*, 1991, **95**, 8881–8886.
- 22 N. Yan, Z.-G. Zhang, Y. Tong, S. Yao, C. Xiao, Z. Li and Y. Kou, *Chem. Commun.*, 2009, 4423–4425.
- 23 J. T. Yates Jr, T. M. Duncan, S. D. Worley and R. W. Vaughan, *J. Chem. Phys.*, 1979, **70**, 1219–1224.
- 24 A. J. Bruss, M. A. Gelesky, G. Machado and J. Dupont, *J. Mol. Catal. A: Chem.*, 2006, **252**, 212–218.
- 25 *Nanoparticles*, ed. G. Schmid, Wiley-VCH, Weinheim, 2004.
- 26 F. Novio, D. Monahan, Y. Coppel, G. Antorrena, P. Lecante, K. Philippot and B. Chaudret, *Chem.-Eur. J.*, 2014, **20**, 1287–1297.
- 27 M. D. Fryzuk and W. E. Piers, in *Organometallic Syntheses*, ed. R. B. King and J. J. Eisch, Elsevier, Amsterdam, 1986, vol. 3, p. 128; W. A. Herrmann, in *Synthetic Methods of Organometallic and Inorganic Chemistry*, ed. W. A. Herrmann, Thieme, Stuttgart, 1996, p. 38.